A PATH PLANNING SCHEME FOR UAV EXPLORER IN CONSIDERATION OF SELF-LOCALIZATION ESTIMATION

Yamato Suzuki[1], Takashi Kubota[2]

[1]The University of Tokyo, 7-3-1 Hongo, Bunkyo-ku, Tokyo, Japan, E-mail: suzuki-yamato304@g.ecc.u-tokyo.ac.jp
[2]JAXA/ISAS, 3-1-1 Yoshinodai, Chuo-ku, Sagamihara, Japan, E-mail: kubota.takashi@jaxa.jp

ABSTRACT

Exploration UAVs (Unmanned Aerial Vehicles) are required to fly autonomously, because GPS cannot be used on Mars. Hence, localization is one of the major topics to be developed. In general, visual odometry is available for relative position estimation. However, it is difficult to estimate absolute position. This paper deals with a path planning in consideration of the absolute localization. This paper introduces Mutual Information for image matching, which is robust to scene changes. MCL (Monte Carlo Localization) is applied for the absolute localization. Then, this paper proposes a new RRT (Rapidly-exploring Random Tree) extension method to generate a path with a large effect of the absolute localization. The simulation results show that the proposed method reduces the uncertainty of the position and generates a path that can increase the probability of reaching the goal.

1 INTRODUCTION

Planetary exploration by robots has contributed to the progressing science [1]. In NASA's Mars 2020 mission, Mars helicopter (Fig. 1) demonstration flights are planned [2]. Autonomous movement in planetary exploration has its own challenges. Since GPS cannot be used on the surface of the planets, position estimation is difficult. Conventional methods for position estimation include Wheel Odometry [3] and Visual Odometry (VO) [4]. Mars helicopter is going to use VO. Since odometry methods are relative position estimation, position errors are accumulated. By using the skyline matching methods [5], absolute position estimation is possible. However, the error is large at several tens of meters. Although there are a few image matching methods [6] for satellite images and UAV equipped camera images, the matching between satellite images with few features and UAV images is difficult. Therefore, it is difficult to exactly reach the goal position when moving while simply performing absolute position estimation based on the images. In such an environment where the position estimation is low accuracy, a path planning algorithm considering the absolute position estimation is required.

Based on the above discussion, this paper proposes a UAV path planning method for improving the accuracy of absolute position estimation in the environments where position estimation is difficult. In the proposed method, RRT [7] is extended under the condition that position uncertainty can be reduced and the error of the position estimation is within the allowable range. As a result, a path with high position estimation accuracy can be generated.

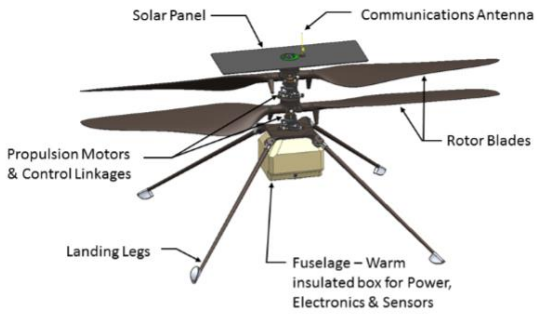

Figure 1: Mars helicopter [2]

The contents of this paper are as follows. Section 2 describes related research. The setting of this research is described in section 3. The proposed method is explained in section 4. Section 5 describes the simulation using satellite images. The simulation results are discussed in section 6. Section 7 gives conclusions and future works.

2 RELATED WORKS

2.1 Absolute Localization

An absolute localization is proposed for UAV by image matching based on satellite images [6]. The proposed method uses mutual information between images is used. This has been shown to be robust to the differences between the images. The Monte Carlo Localization (MCL) is applied to the image matching method [8].

2.2 Path Planning

So far, there have been no research on path planning considering absolute localization for the exploration UAVs. The path planning considering VO [9] and the path planning aimed at suppressing the uncertainty of

relative localization [10] have been proposed for the planetary exploration rovers. Regarding the drones, the path planning method that consider image features have also been studied [11]. These methods cannot consider absolute localization in the satellite image.

The path planning methods considering absolute localization have also been proposed. A path planning method considering GPS area and non-GPS area is proposed [12]. However, it is not possible to use a method such as GPS that can reliably estimate absolute position within the predetermined areas for Mars exploration. A path planning method considering absolute localization for the planetary exploration rovers is also proposed [13]. The Kalman Filter measurement update step is used for absolute localization. There is an assumption that the uncertainty can be always reduced in the Kalman Filter measurement update step. However, when the difference between the satellite image and the UAV camera image is large, there is a problem that the uncertainty cannot always be reduced by the absolute localization based on the images.

3 PROBLEM SETTING

3.1 Image Matching Method

In this paper, MCL is applied to image matching using mutual information between images to represent absolute localization. Here, the mutual information between images will be described. When obtaining the mutual information between images, it is assumed that the two images are monochrome images of the same size. The probability distribution function $P_I(i)$ for intensity value *i* existing in the image *I* is defined by Eq. 1.

$$P_I(i) = \frac{1}{N}\sum_x \delta\big(i - I(x)\big) \tag{1}$$

, where $P_I(i)$ represents the probability that the intensity value i = 0, 1, 2, …, 255 appears in the image *I*. $\boldsymbol{x}$ denotes a two dimensional vector of integers representing discrete pixel positions in image *I*. *N* denotes the number of pixels in the image *I*, and $I(\boldsymbol{x})$ denotes the intensity value of the pixel at $\boldsymbol{x}$, respectively. $\delta()$ denotes the Kronecker delta function defined by Eq. 2.

$$\delta(i - i') = \begin{cases} 1\ (i = i') \\ 0\ (i \neq i') \end{cases} \tag{2}$$

Similarly, the joint probability distribution of the images *I* and *I'* of the same size is defined by Eq. 3.

$$P_{II'}(i,j) = \frac{1}{N}\sum_x \delta\big(i - I(x)\big)\delta\big(j - I'(x)\big) \tag{3}$$

where *i* and *j* represent intensity value of 0, 1, 2, …, 255. At this time, the mutual information (MI) between images is obtained by Eq. 4.

$$\mathrm{MI}[I, I'] = \sum_{i=0}^{255}\sum_{j=0}^{255} P_{II'}(i,j)\log\frac{P_{II'}(i,j)}{P_I(i)P_{I'}(j)} \tag{4}$$

In this paper, the mutual information between images is calculated by using Eq. 4.

3.2 UAV Images during Path Planning

Referring to [2], the UAV is equipped with a vertically downward grayscale camera (image size 640×480), altimeter, IMU, and inclinometer. In this paper, it is assumed that the yaw angle is also obtained by the sun sensor. From this information, this paper assumes that the UAV attitude roll, pitch, yaw, and altitude z are known and constant.

It is assumed that the satellite image is a monochrome satellite image $I_{\mathrm{satellite}}$ of 0.25 m/pixel. The lower the altitude of the UAV, the higher the resolution of the image that can be obtain. This paper assume that the image obtained by the UAV camera is I_u^* and the resolution of the image I_u^* is 0.025 m/pixel, which is 10 times different from the satellite image. The actual exploration UAV 1/10 downsamples the image I_u^* and adjusts the resolution to 0.25 m/pixel, obtains an image I_u of size 64×48 and matches it with the satellite image. Let l_u and w_u be the vertical and horizontal pixel numbers of the UAV image I_u, respectively. In this paper w_u is 64, and l_u is 48. Let $I_s(x,y)$ be the image trimmed with the size $w_u \times l_u$ at the coordinates (x,y) in the satellite image $I_{\mathrm{satellite}}$. At this time, the mutual information between images at the coordinates (x,y) in the satellite image $I_{\mathrm{satellite}}$ can be defined as Eq. 5 using Eq. 4.

$$\mathrm{MI}(x,y) = \mathrm{MI}[I_u, I_s(x,y)] \tag{5}$$

Eq. 5 represents the similarity. The position $(\hat{x},\hat{y})$ in the satellite image where the value of Eq. 5 is maximized can be calculated by the following equation.

$$(\hat{x},\hat{y}) = \arg\max_{(x,y)} \mathrm{MI}(x,y) \tag{6}$$

The absolute position of the UAV can be identified by Eq. 5 and Eq. 6 if the difference between the UAV image and the satellite image is small. However, it is not possible to obtain the UAV camera image I_u^* with higher resolution than the satellite image at the stage of path planning performed in advance. Therefore, the image I_u cannot be obtained by downsampling. In addition, when flying at low altitudes, the difference in resolution becomes large, making absolute localization difficult. In order to reproduce the difference between the images, this proposed method prepares an image I_{world} in which the intensity value of each pixel of the image $I_{\text{satellite}}$ is added with Gaussian noise with mean 0 and standard deviation σ_{img}. At the true position $\boldsymbol{x}_{\text{true}} = (x_{\text{true}}, y_{\text{true}})$, the image trimmed from the image I_{world} with a size of 64 × 48 after 1/10 downsampling is regarded as the UAV image I_u. The image I_u obtained by the UAV as a camera image is regarded as being matched to the resolution of the satellite image $I_{\text{satellite}}$. At this time, $\boldsymbol{x}_{\text{true}}$ represents the upper left corner of the image I_u.

4 PROPOSED PATH PLANNING METHOD

4.1 Uncertainty in Path Planning

There are two ways to represent the uncertainty in path planning: ellipse approximation like Kalman Filter [12][14] and particle representation like Particle Filter [10]. In [10], the uncertainty increases monotonically because the absolute localization is not considered.

In this paper, the propagation of the uncertainty is briefly expressed using confidence ellipse approximation. On the other hand, particle representation is used for absolute localization. Namely, Particle Filter Localization (Monte Carlo Localization, MCL) is used for the absolute localization. In ellipse approximation such as the Kalman Filter, there is an assumption that the uncertainty is always reduced in the measurement update step. In this paper, this assumption becomes unnecessary by using the particle representation for the measurement update step, that is, the absolute localization. In this way, it is possible to quantitatively represents the increase or decrease of the uncertainty in absolute localization.

4.2 RRT considering Confidence and Reliability of Absolute Localization

Algorithm 1 shows the proposed RRT-based path planning method (Confidence-Reliability-Aware RRT, CRA-RRT) which considers the confidence and reliability of the absolute localization based on images. Algorithm 2 represents the function SelectMinCostNode() in Algorithm 1. This function selects the candidate point for RRT extension that can be reduced the uncertainty, has the estimated position within the allowable range and has the minimum cost. Unlike related works, this algorithm can consider the increase or decrease in the uncertainty of absolute localization and the reliability of the estimated position.

The outline of the proposed method is as follows. In CRA-RRT, the n_{near} nearest nodes in RRT graphs with respect to $\boldsymbol{x}_{\text{rand}}$ are defined as $v_{\text{near}} \in V_{\text{near}}$. Let $v_{\text{candidate}}.\boldsymbol{x}$ be the point extended by a certain distance l_e from $v_{\text{near}}.\boldsymbol{x}$. Save the value that propagates the uncertainty from v_{near} to $v_{\text{candidate}}$ in the candidate node $v_{\text{candidate}}$. Let $V_{\text{candidate}}$ be a set of the n_{near} candidate nodes. At these candidate nodes $v_{\text{candidate}} \in V_{\text{candidate}}$, the uncertainty can be reduced by MCL, the error of the estimated position is within the allowable range $\varepsilon_{\text{threshold}}$, and the node with the minimum cost is adopted as new RRT node. As a result, it is possible to increase the confidence by reducing the uncertainty and improve the reliability of the estimated position.

4.3 Uncertainty Quantification

This section defines the quantity that represents position uncertainty. The average of the positions of the particles $\hat{x}$ and the covariance matrix $\boldsymbol{\Sigma}$ are represented by Eq. 7 and Eq. 8, respectively.

$$\hat{\boldsymbol{x}} = \frac{1}{M}\sum_{i=1}^{M} \boldsymbol{x}^i_{\text{particle}} \tag{7}$$

$$\boldsymbol{\Sigma} = \frac{1}{M}\sum_{i=1}^{M} \left(\boldsymbol{x}^i_{\text{particle}} - \hat{\boldsymbol{x}}\right)\left(\boldsymbol{x}^i_{\text{particle}} - \hat{\boldsymbol{x}}\right)^T \tag{8}$$

Eq. 7 represents the estimated position. The uncertainty value proportional to the area of the confidence ellipse is defined by Eq. 9.

$$S_{\text{uncertainty}} = \sqrt{\det(\boldsymbol{\Sigma})} \tag{9}$$

4.4 Uncertainty Propagation in Path Planning

The propagation of the uncertainty associated with the motion in the proposed method is briefly represented by using confidence ellipse approximation similar to [14]. Let $v_{\text{candidate}}.\boldsymbol{\Sigma}$ be the propagation of the uncertainty $v_{\text{near}}.\boldsymbol{\Sigma}$ of each nearest neighbor node $v_{\text{near}} \in V_{\text{near}}$ of the sampled point $\boldsymbol{x}_{\text{rand}}$. Then $v_{\text{candidate}}.\boldsymbol{\Sigma}$ can be calculated by Eq. 10 and Eq. 11.

Algorithm 1 Confidence-Reliability-Aware RRT

Input: Satellite image $I_{\text{satellite}}$, initial position $\boldsymbol{x}_{\text{init}}$, initial uncertainty $\boldsymbol{\Sigma}_{\text{init}}$, goal position $\boldsymbol{x}_{\text{goal}}$ and goal region $\boldsymbol{X}_{\text{goal}}$

$I_{\text{world}} \leftarrow \text{CreateVirtualWorldImage}(I_{\text{satellite}})$
$v.\boldsymbol{x} \leftarrow \boldsymbol{x}_{\text{init}}$; $v.\hat{\boldsymbol{x}} \leftarrow \boldsymbol{x}_{\text{init}}$; $v.\boldsymbol{\Sigma} \leftarrow \boldsymbol{\Sigma}_{\text{init}}$; v.PathLength $\leftarrow 0$; v.Parent $\leftarrow$ NULL;
$V \leftarrow \{v\}$
while True **do**
$\boldsymbol{x}_{\text{rand}} \leftarrow \text{Sample}(I_{\text{satellite}})$
$V_{\text{near}} \leftarrow \text{NearestNeighbors}(V, \boldsymbol{x}_{\text{rand}}, n_{\text{near}})$
$V_{\text{candidate}} \leftarrow \text{CreateNewNodes}(n_{\text{near}})$
$V_{\text{candidate}} \leftarrow \text{Propagate}(V_{\text{near}}, \boldsymbol{x}_{\text{rand}}, l_e)$
$c_{\text{min}} \leftarrow \infty$
$v_{\text{min}} \leftarrow v$
$(c_{\text{min}}, v_{\text{min}}) \leftarrow \text{SelectMinCostNode}(c_{\text{min}}, v_{\text{min}}, V_{\text{candidate}}, I_{\text{satellite}}, I_{\text{world}})$
if $c_{\text{min}} < \infty$ **then**
$V \leftarrow V \cap \{v_{\text{min}}\}$
if $v_{\text{min}}.\boldsymbol{x} \in \boldsymbol{X}_{\text{goal}}$ **then**
return V
end if
end if
end while

$$v_{\text{candidate}}.\boldsymbol{\Sigma} = v_{\text{near}}.\boldsymbol{\Sigma} + \boldsymbol{R}_{\text{unc}} \tag{10}$$

$$\boldsymbol{R}_{\text{unc}} = \text{diag}\left(\left(\alpha_{\text{uncertainty}} l_e\right)^2, \left(\alpha_{\text{uncertainty}} l_e\right)^2\right) \tag{11}$$

, where l_e is the internode distance.

4.5 Cost Function

The cost function at the candidate node $v_{\text{candidate}}$ is defined by the Eq. 12

$$\begin{aligned}&\text{Cost}(v_{\text{candidate}}) \\ &= w_d\left(v_{\text{candidate}}.\text{PathLength} \right. \\ &\left. + \text{H}(v_{\text{candidate}}.\boldsymbol{x})\right) + w_u\, S^{\text{after}}_{\text{uncertainty}}\end{aligned} \tag{12}$$

Algorithm 2 Select Minimum Cost Node

Input: Minimum cost c_{min}, minimum cost node v_{min}, candidate nodes set $V_{\text{candidate}}$, satellite image $I_{\text{satellite}}$, virtual world image I_{world}

for all $v_{\text{candidate}} \in V_{\text{candidate}}$ **do**
$I_u \leftarrow \text{GetImg}(I_{\text{world}}, \text{Size}(I_u), v_{\text{candidate}}.\boldsymbol{x})$
$\boldsymbol{X}_{\text{particle}} \leftarrow \emptyset$; $\boldsymbol{W}_{\text{particle}} \leftarrow \emptyset$;
for $i \leftarrow 1$ to n_{particle} **do**
$\boldsymbol{x}^i_{\text{particle}} \sim \mathcal{N}(v_{\text{candidate}}.\boldsymbol{x}, v_{\text{candidate}}.\boldsymbol{\Sigma})$
$\boldsymbol{X}_{\text{particle}} \leftarrow \boldsymbol{X}_{\text{particle}} \cap \{\boldsymbol{x}^i_{\text{particle}}\}$
$I_s \leftarrow \text{GetImg}(I_{\text{satellite}}, \text{Size}(I_u), \boldsymbol{x}^i_{\text{particle}})$
$w^i \leftarrow \text{CalcSimilarity}(I_u, I_s)$
$\boldsymbol{W}_{\text{particle}} \leftarrow \boldsymbol{W}_{\text{particle}} \cap \{w^i\}$
end for
$S^{\text{before}}_{\text{uncertainty}} \leftarrow \text{CalcUncertainty}(\boldsymbol{X}_{\text{particle}})$
$\boldsymbol{X}_{\text{particle}} \leftarrow \text{Resample}(\boldsymbol{X}_{\text{particle}}, \boldsymbol{W}_{\text{particle}})$
$S^{\text{after}}_{\text{uncertainty}} \leftarrow \text{CalcUncertainty}(\boldsymbol{X}_{\text{particle}})$
$(v_{\text{candidate}}.\hat{\boldsymbol{x}}, v_{\text{candidate}}.\boldsymbol{\Sigma}) \leftarrow \text{MeanCov}(\boldsymbol{X}_{\text{particle}})$
$\varepsilon \leftarrow \text{Distance}(v_{\text{candidate}}.\boldsymbol{x}, v_{\text{candidate}}.\hat{\boldsymbol{x}})$
$c \leftarrow \text{Cost}(v_{\text{candidate}})$
If $S^{\text{before}}_{\text{uncertainty}} > S^{\text{after}}_{\text{uncertainty}}$ and $\varepsilon_{\text{threshold}} > \varepsilon$ and $c_{\text{min}} > c$
$c_{\text{min}} \leftarrow c$
$v_{\text{min}} \leftarrow v_{\text{candidate}}$
end if
end for
return $(c_{\text{min}}, v_{\text{min}})$

, where $v_{\text{candidate}}.\text{PathLength}$ is the path length from the start position to the candidate node position $v_{\text{candidate}}.\boldsymbol{x}$, $\text{H}(v_{\text{candidate}}.\boldsymbol{x})$ is the shortest distance from the candidate node position $v_{\text{candidate}}.\boldsymbol{x}$ to the goal position, and w_d and w_u are the weights related to the path length and the uncertainty, respectively. These weights are set so that $w_d + w_u = 1, w_d \geq 0, w_u \geq 0$. By setting the weight parameters by the user of the path planning method, it is possible to generate a path considering

the balance between the magnitude of the effect of absolute localization and the path length.

5 SIMULATION STUDY

5.1 Simulation Setting

Fig. 2 shows the satellite image ESP_062319_1985 [15] of the candidate landing site for the Mars 2020 mission obtained from NASA's HiRISE Mars probe camera. The monochrome version of this image is defined as the satellite image $I_{\text{satellite}}$ in the simulation. The intensity value of each pixel is an integer from 0 to 255. In Fig. 2, the start position (100, 130) is indicated by a blue dot, the goal position (700, 130) is indicated by a red dot, and the goal area is indicated by a red circle. These are used as inputs for the path planning algorithm, and the paths are output and saved. This section will evaluate the path planning method by path following simulations.

The simulation parameters are shown in Tab. 1. The goal sampling rate r_g is the probability of sampling the goal position during random sampling. This allows users of the RRT path planning algorithm to set the search probability in the goal direction. It is assumed that the initial true position is generated from the Gaussian distribution with the start position as the mean and with the standard deviation of σ_{true}. The belief distribution at the initial position is the mean of the start position, and the uncertainty is the covariance matrix with the standard deviation of σ_{init}. In this simulation, the minimum uncertainty σ_{min} is set to prevent the absolute localization from becoming impossible due to the belief distribution becoming too small. The motion uncertainty is represented by α, which represents the magnitude of uncertainty per distance traveled. In this simulation, the parameter of the belief distribution is set twice as large as the true value with respect to the magnitude of uncertainty in order to prevent the estimation of the position from becoming impossible. α_{true} is the magnitude of uncertainty of the true position per travel distance. If $\alpha_{\text{true}} = 0.05$, it means that the uncertainty of 5% of the distance traveled is added. Let $\boldsymbol{u}(t)$ be the vector from the estimated position after the absolute localization at a certain time step t to the next target position. Let $\boldsymbol{R}_{\text{true}}(t)$ be the motion uncertainty of the true position. At this time, the motion of the true position is represented by Eqs. 13-15.

$$\boldsymbol{x}_{\text{true}}(t+1) = \boldsymbol{x}_{\text{true}}(t) + \boldsymbol{u}(t) + \boldsymbol{w}_{\text{true}}(t) \quad (13)$$

$$\boldsymbol{w}_{\text{true}}(t) \sim \mathcal{N}\left(\boldsymbol{0}, \boldsymbol{R}_{\text{true}}(t)\right) \quad (14)$$

Figure 2: Start position (blue), goal position (red) and goal area (red circle) in the satellite image [15] by NASA/JPL/University of Arizona

Table 1: Parameters for simulation

Parameter type	Symbol	Value
Particles	n_{particle}	500
Nearest Neighbors	n_{near}	5
Step size	l_e	10 [pixel]
Goal sampling rate	r_g	5 [%]
Minimum uncertainty	σ_{min}	4.03 [pixel]
Initial uncertainty of true position	σ_{true}	4.03 [pixel]
Initial uncertainty	σ_{init}	8.06 [pixel]
Motion uncertainty of true position	α_{true}	0.05
Motion uncertainty	$\alpha_{\text{uncertainty}}$	0.10
Image noise	σ_{img}	10

$$\boldsymbol{R}_{\text{true}}(t) = \text{diag}((\alpha_{\text{true}}\|\boldsymbol{u}(t)\|)^2, (\alpha_{\text{true}}\|\boldsymbol{u}(t)\|)^2) \quad (15)$$

The true position is unknown for the UAV when following the path. On the other hand, the current estimated position and the next target position are known. Namely, the vector $\boldsymbol{u}(t)$ is known. Therefore, Eq. 13 represents that the true position is moved from the current position to the next target position with uncertainty. The propagation of the belief distribution accompanying the motion of the UAV is represented by Eqs. 16-18.

$$\bar{\boldsymbol{x}}(t+1) = \hat{\boldsymbol{x}}(t) + \boldsymbol{u}(t) \quad (16)$$

$$\bar{\Sigma}(t+1) = \Sigma(t) + \boldsymbol{R}_{\text{unc}}(t) \quad (17)$$

$$\boldsymbol{R}_{\text{unc}}(t) = \text{diag}\left(\left(\alpha_{\text{uncertainty}}\|\boldsymbol{u}(t)\|\right)^2, \left(\alpha_{\text{uncertainty}}\|\boldsymbol{u}(t)\|\right)^2\right) \quad (18)$$

, where $\bar{\boldsymbol{x}}(t+1)$ is the estimated position after the motion. This matches the target position. $\hat{\boldsymbol{x}}(t)$ is the estimated position of the node at time step t, $\bar{\Sigma}(t+1)$ is the uncertainty of the belief distribution after the motion, $\Sigma(t)$ is the uncertainty of the node at time step

t, $\alpha_{\text{uncertainty}}$ is the magnitude of uncertainty per travel distance of the belief distribution. In addition, when the difference between the satellite image and the UAV camera image is large, the true position and the position identification result of Eq. 6 may not match. In order to reproduce such a situation, the standard deviation at the time of image I_{world} generation is set to $\sigma_{\text{img}} = 10$ so that there are some cases that the true position $\boldsymbol{x}_{\text{true}}$ and the identification result of Eq. 6 do not match.

5.2 Simulation Evaluation Method

As the evaluation value, the goal reach rate of the true position and the final uncertainty are used. The goal reach rate represents the probability that the true position is reached the goal area when the estimated position is reached the goal area. The final uncertainty is the uncertainty when the estimated position is reached the goal area. The smaller the final uncertainty, the higher the confidence of self-position, and the higher goal reach rate, the higher the reliability of absolute localization.

The method of deriving the evaluation value of the path planning method is described as follows. First, generate 30 paths for a certain condition. For each generated path, the path is followed 100 times, the number of the true position reaching the goal area is measured, and the number is divided by 100 to derive the goal reach rate. The final uncertainty is calculated by following 100 times for each path, obtaining the final uncertainty at 100 times goals, taking the average, and taking the average for the 30 paths. These goal reach rate and final uncertainty are used as evaluation values in this simulation.

Next, the evaluation method of the best path regarding the goal reach rate of the paths generated by the proposed method CRA-RRT and the best path in the sense of the shortest path generated by the normal RRT method is described. The path with the highest goal reach rate among the 30 paths generated by the proposed method is set as the best path regarding the goal reach rate. The straight path generated by the normal RRT when the goal sampling rate r_g = 100% is the best path in the sense of the shortest path. This simulation compares the goal reach rate and the average value of the final uncertainty when 500 path-following simulations are performed for each of these paths.

6 SIMULATION RESULTS

6.1 Comparison for Parameter Changes

In the proposed method, the comparison results are shown for the results when the parameters are changed. When the reliability threshold $\varepsilon_{\text{threshold}} = \infty$ and the weight parameters of the cost function are $(w_d, w_u) = (1.0,0.0), (0.5,0.5), (0.0,1.0)$, the goal reach rate results are shown in Fig. 3. The results when $\varepsilon_{\text{threshold}} = 0.5$ are shown in Fig. 4. Similarly, the final uncertainty results are shown in Fig. 6 and Fig. 7. It was shown that the larger the weight parameter w_u, the higher the goal reach rate and the smaller the final uncertainty. It was also shown that the smaller the tolerance $\varepsilon_{\text{threshold}}$ of the estimated position, the higher the goal reach rate and the smaller the uncertainty. In Fig. 4, the change in goal reach rate is small because if $\varepsilon_{\text{threshold}}$ is very small, there are almost no candidate nodes that satisfy the reliability condition of the estimated position, and the cost cannot be considered.

6.2 Comparison of Path Planning Method

Next, a comparison between the normal RRT (goal sampling rate r_g = 5%) and the proposed method is shown. Tab. 2 shows the evaluation results. This simulation uses $\varepsilon_{\text{threshold}} = 0.5, (w_d, w_u) = (0.0,1.0)$ as the parameter when generating the paths by the proposed method. As a path planning method, normal RRT adopts nodes as it is without considering the effect of absolute localization. As a result, it is considered that the effect of absolute localization was small even when the path was followed while performing absolute position estimation. Consequently, the goal reach rate of normal RRT was low, and the final uncertainty was large.

6.3 Comparison of the Best Paths

Finally, this simulation compares the performance of the straight path, which is the shortest path, and the path with the maximum goal reach rate among the 30 paths generated by the path planning algorithm of the proposed method, CRA-RRT. Tab. 3 shows the evaluation results. The best path by the proposed method improved the goal reach rate by 18.4% and reduced the final uncertainty by 58.9% from 135 to 55.5 on average compared to the straight path. Fig. 7 and Fig. 8 show the straight path and the path of CRA-RRT with the maximum goal reach rate, respectively. The white dots in Fig. 7 and Fig. 8 represent the positions where the UAV obtains an image when the path is perfectly followed. Here, the white dots are the dots at the upper left corner of the UAV image. If the UAV go along the straight path from the start to the goal, the UAV will pass through a feature-poor terrain. The path generated by the proposed method in Fig. 8 was planned to bypass the feature-poor terrain.

7 CONCLUSION

This paper proposed a path planning method aimed at

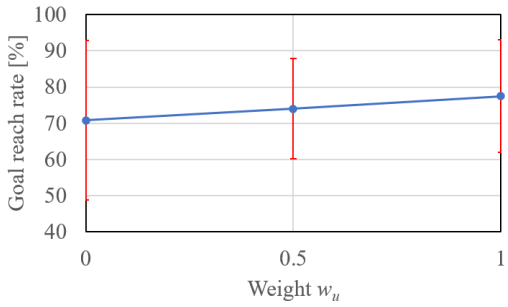

Figure 3: Goal reach rate ($\varepsilon_{\text{threshold}} = \infty$)

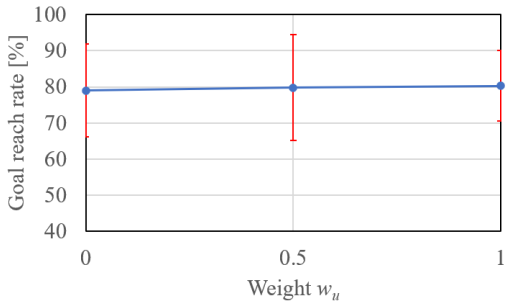

Figure 4: Goal reach rate ($\varepsilon_{\text{threshold}} = 0.5$)

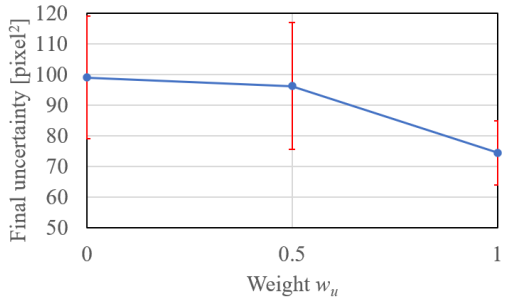

Figure 5: Final uncertainty ($\varepsilon_{\text{threshold}} = \infty$)

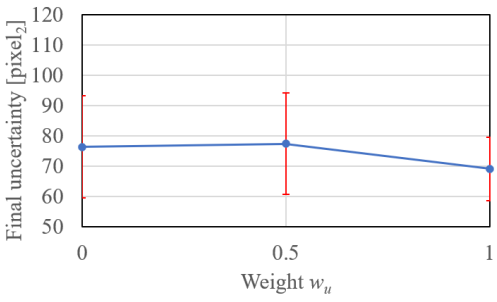

Figure 6: Final uncertainty ($\varepsilon_{\text{threshold}} = 0.5$)

Table 2: Comparison of RRT and CRA-RRT

	RRT	CRA-RRT
Goal reach rate [%]	58.5 ± 19.7	80.4 ± 9.74
Final uncertainty [pixel^2]	98.9 ± 26.9	69.1 ± 10.5

Table 3: Comparison of the straight path and the CRA-RRT path

	Straight path	CRA-RRT
Goal reach rate [%]	74.4	92.8
Final uncertainty [pixel^2]	135 ± 70.8	55.5 ± 15.9

improving the absolute localization accuracy for the exploration UAVs. By extending the path by quantitatively considering the increase or decrease of the uncertainty in absolute localization and the error of position estimation, the confidence and the reliability of position estimation were improved. The effectiveness of the proposed method was shown by simulations.

A future work is to realize a three-dimensional path planning. In this paper, it is assumed that the altitude is constant, however, it is desirable to build a model of position estimation that changes three-dimensionally and apply it to the proposed method to build a more practical path planning method.

References

[1] J.P. Grotzinger et al. (2012). Mars science laboratory mission and science investigation, Space Science Reviews, 170(1-4), 5-56.

[2] D.S. Bayard et al. (2019). Vision-based navigation for the NASA mars helicopter, AIAA Scitech 2019 Forum.

[3] R. Li et al. (2004). Rover localization and landing-site mapping technology for the 2003 mars exploration rover mission, Photogrammetric Engineering and Remote Sensing, pp.77-90.

[4] M. Maimone et al. (2007). Two years of visual odometry on the mars exploration rovers, Journal of Field Robotics, 24(3), 169-186.

[5] F. Cozman et al. (2000). Outdoor visual position estimation for planetary rovers, Autonomous Robotics, vol.9, pp.135-150.

[6] A. Yol et al. (2014). Vision-based absolute localization for unmanned aerial vehicles, IEEE/RSJ International Conference on Intelligent Robots and Systems, pp.3429-3434.

[7] S.M. LaValle and J.J. Kuffner Jr. (2001). Randomized kinodynamic planning, The international journal

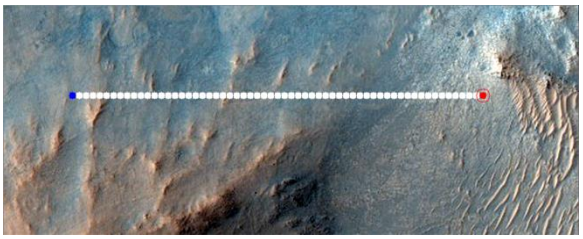

Figure 7: Straight path (shortest path) in the satellite image [15]

Figure 8: Highest goal reach rate path in the satellite image [15]

of robotics research, 20(5), 378-400.

[8] L.D.P. Veronese et al. (2015). Re-emission and satellite aerial maps applied to vehicle localization on urban environments, IEEE/RSJ International Conference on Intelligent Robots and Systems, pp.4285-4290.

[9] K. Otsu et al. (2018). Where to look? Predictive perception with applications to planetary exploration, IEEE Robotics and Automation Letters, 3(2), 635-642.

[10] M. Mizuno and K. Kubota. (2019). Path planning considering motion uncertainty for exploration robots in natural terrain, Journal of the Robotics Society of Japan, 37(7), 639-645, (in Japanese).

[11] S.A. Sadat et al. (2014). Feature-rich path planning for robust navigation of MAVs with mono-SLAM, IEEE International Conference on Robotics and Automation, pp.3870-3875.

[12] S.U. Lee et al. (2016). Robust sampling-based motion planning for autonomous tracked vehicles in deformable high slip terrain, IEEE International Conference on Robotics and Automation, pp.2569-2574.

[13] E. Fang et al. (2019). Belief space planning for reducing terrain relative localization uncertainty in noisy elevation maps, International Conference on Robotics and Automation, pp.4753-4759.

[14] A. Bry and N. Roy. (2011). Rapidly-exploring random belief trees for motion planning under uncertainty, IEEE International Conference on Robotics and Automation, pp.723-730.

[15] NASA/JPL/University of Arizona. ESP_062319_1985, https://www.uahirise.org/ESP_062319_1985, [Accessed: 16- September- 2020].